Three-dimensional optical modeling and optimizations of color filter liquid-crystal-on-silicon microdisplays

Baolong Zhang, Hoi-Sing Kwok, and Ho-Chi Huang[a)]
Department of Electrical and Electronic Engineering, The Hong Kong University of Science and Technology, Clear Water Bay, Kowloon, Hong Kong

(Received 29 June 2005; accepted 9 November 2005; published online 28 December 2005)

We have developed a three-dimensional (3D) optical modeling of small color pixels in color filter liquid-crystal-on-silicon (CF-LCOS) microdisplays. The 3D optical modeling includes a LC electromechanical analysis of color LC cells, a calculation of optical reflectance using the extended Jones matrix, and a standard RGB (sRGB) representation of the optical reflectance in the pixel array. The simulated optical reflectance agreed well with the experiments. With this 3D optical analysis as a tool, the relation of the lateral color fringing field with pixel size and thickness of color filter were studied. Minimizations of the fringing field in the CF-LCOS microdisplays were obtained by pixel arrangement, rubbing direction, and LC mode. The color purity of the CF-LCOS microdisplays could attain 63% National Television System Committee (NTSC) level for a typical pixel size of 15 μm. With an optimized LC mode, the color purity could still be maintained at 54% NTSC level even when the pixel size was reduced to 9 μm. This enabled the feasibility of the CF-LCOS microdisplays for very high-resolution display applications. © *2005 American Institute of Physics*. [DOI: 10.1063/1.2149494]

I. INTRODUCTION

We have developed a practical color filter liquid-crystal-on-silicon (CF-LCOS) microdisplay that integrated color filters on silicon for color.[1,2] The projection or viewing optics of this breed of microdisplays is greatly simplified since color is already available. What it needs is just a polarizing beam splitter (PBS) to direct a polarized light into the display and back to a projection lens or eyepiece. In this paper, we present optical modeling and optimizations of the CF-LCOS microdisplays.

In our previous works, we have developed a two-dimensional (2D) optical modeling of small pixels in reflective twisted nematic cells.[3] In this work, we added color filters in the simulation structures and elaborated the 2D modeling to three dimensions. The three-dimensional (3D) optical analysis started with a numerical calculation of LC director in rectangular mesh. Thereafter we calculated for optical reflectance of color pixels in the visible spectrum by extended Jones matrix. The optical reflectance spectrum was then converted to the CIE 1931 color space for color coordinate, which was a good measure of color purity. The optical reflectance was also expressed spatially by the sRGB[4] format in the pixel array, so the color fringing field among small color pixels could be visualized. With this analysis as a tool, we proceeded to minimize the color fringing field with respect to pixel arrangement, rubbing direction, and LC mode. We also studied the relation of color fringing field with pixel size and thickness of color filter, and optimized the CF-LCOS microdisplays for specific applications.

[a)]Author to whom correspondence should be addressed; electronic mail: eehuang@ust.hk

II. 3D OPTICAL MODELING

A. LC electromechanical analysis

The first step of the 3D optical modeling is the LC electromechanical analysis. The purpose of the LC electromechanical analysis is to determine the LC director as a function of the applied voltage of the LC cell. The LC director can be obtained numerically by solving the Poisson equation and a continuum theory equation with the method of successive over relaxation (SOR).[5,6] The Poisson equation describes the potential distribution $V(x,y,z)$ with respect to the anisotropic dielectric constant of the LC cell as follows:

$$\nabla[\vec{\vec{\varepsilon}}(x,y,z)\,\nabla\,V(x,y,z)]=0, \tag{1}$$

where $\vec{\vec{\varepsilon}}(x,y,z)$ is the dielectric constant tensor of the LC cell and its component $\varepsilon_{ij}(x,y,z)$ can be expressed as

$$\varepsilon_{ij}(x,y,z)=\varepsilon_v\delta_{ij}+(\varepsilon_p-\varepsilon_v)n_i(x,y,z)n_j(x,y,z). \tag{2}$$

In Eq. (2), δ_{ij} is the delta function, ε_p and ε_v are the dielectric constants parallel and perpendicular to the LC director, and n_i and n_j are components of the LC director **n** projected onto the i and j axes, respectively, where i and j are any two of x, y, and z. The 3D LC director **n** can be solved from a continuum theory equation as follows:

$$\gamma\frac{\partial n_i}{\partial t}=\frac{d}{d_j}\left[\frac{\partial(F_s-F_e)}{\partial(\partial n_i/\partial j)}\right]-\frac{\partial(F_s-F_e)}{\partial n_i}, \tag{3}$$

where γ is the rotational viscosity, F_s and F_e are the elastic and electrostatic energy density functions, respectively,[7] and can be further expressed as

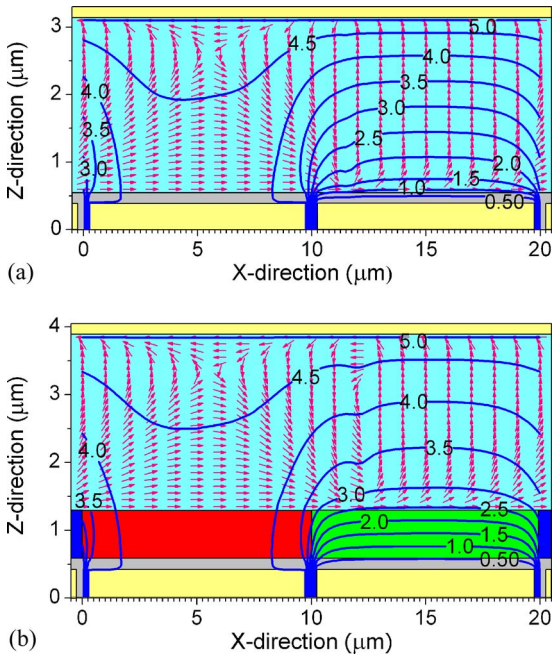

FIG. 1. (Color online) Cross section of the 3D director of (a) the monochrome and (b) color LC cells.

$$F_s = \frac{1}{2}K_{11}(\nabla \cdot \mathbf{n}) + \frac{1}{2}K_{22}(\mathbf{n} \cdot \nabla \times \mathbf{n} + q_0)^2 + \frac{1}{2}K_{33}|(\mathbf{n} \times \nabla \times \mathbf{n})|^2, \quad (4)$$

and

$$F_e = \varepsilon_o \mathbf{E} \cdot \varepsilon \mathbf{E}, \quad (5)$$

where $\mathbf{n}=[n_x, n_y, n_z]$ is the LC director vector, q_0 is the chiral dopant, $\mathbf{E}$ is the electric field vector, and K_{11}, K_{22}, and K_{33} are the splay, twist, and bend coefficients of the LC mixture, respectively.

We applied the LC electromechanical analysis to the 3D simulation structures of monochrome and color LC cells whose cross sections are shown in Fig. 1. Both the monochrome and color LC cells were in a mixed-mode twisted nematic (MTN) configuration,[8] in which the twisted angle was 90°, the polarizer angle was 20°, the pretilt angle was 2°, and the rubbing angle was 45° with respect to the pixel edge. The cell gap or the thickness of the LC layer was 2.5 μm and a LC mixture, MLC-6043 from Merck, with a retardation of 0.1 was used for simulation.

Periodic boundary conditions were applied on both the left and right edges, at which the LC director, potential, and their derivatives were continuous horizontally. In the vertical direction, the electric displacement was continuous through the color filter and LC layers, and finally a strong anchoring energy was assumed for the LC alignment. The color cell had a 0.75 μm color filter layer below the LC layer and above the pixel electrodes. With dielectric constants and resistivity of color filters characterized and available,[1,2] we were able to simulate for the electromechanical properties of the color LC cell.

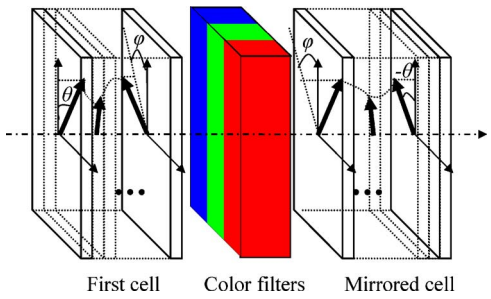

FIG. 2. (Color online) The optical reflectance model of the reflective color pixels.

There were three electrodes in the cross section of the simulation structures as shown in Fig. 1. The common voltage on the top glass plate was kept at a constant voltage of 5 V. The bottom two pixel electrodes were varied from 0 to 4 V and resulted in a root-mean-squared voltage of 5 to 1 V across the top and bottom electrodes. In this arrangement, the LC cells were driven in frame inversion, where the lateral fringing field was relatively small in comparison with that in column or row inversion. This small fringing field is negligible in the monochrome microdisplays in which the lateral fringing field would only alter the area of brightness or darkness of the neighboring pixels. It would not affect the overall brightness and contrast. But the small fringing field in frame inversion cannot be ignored in the CF-LCOS microdisplays because the neighboring pixels have different colors. The alternation of the area of brightness or darkness of the neighboring pixels would cause color leakage and degrade greatly the color saturation of the display.

In the electromechanical analysis, we divided the LC cell into 50 layers and set the iteration tolerance of the simulation to 1.0×10^{-6}. With these parameters, convergent numerical results of the 3D LC director and potential were obtained. The electric filed, which is the negative gradient of the potential distribution in the LC layers, could also be obtained. The difference of the director $\Delta n(x,y,z)$ and potential $\Delta V(x,y,z)$ between neighboring LC layers were less than 0.01 and 50 μV, respectively. The cross section of the simulated 3D LC director was already shown in the simulation structures of Fig. 1. The bottom pixel electrodes were 4 and 0 V, respectively, to create the largest lateral fringing field in frame inversion. Since the applied voltage was partially dropped in the color filters, the lateral electric field extended more into the color pixels than into the monochrome pixels. This implied that the color cell had a more severe fringing effect than that of the monochrome one.

B. Optical reflectance analysis

With the 3D LC director available from the LC electromechanical analysis, and optical constants of the color filters available from the optical characterizations,[1,2] we were able to calculate for the optical reflectance of the color LC cell in the visible spectrum by the extended Jones matrix.[9] We modeled the reflective color pixels by a transmittive LC cell, a color filter layer, and a mirrored transmittive LC cell of the first one in series as shown in Fig. 2. The color filters were represented by absorptive and isotropic media. The LC cells

were divided into a stack of N birefringent plates in which each plate was twisted slightly from its neighbors. N was 50, the same as the number of LC layers used in the electromechanical analysis. The optical axis was regarded as fixed within each plate and the LC element was treated as a uniaxial medium sandwiched between two isotropic media. In this condition, we considered only the **s** and **p** vectors of the incident wave and represented the optical transmission by its ordinary and extraordinary components.

The refraction of light at the interface of the isotropic and uniaxial media is expressed in a matrix form as

$$\begin{bmatrix} E_e' \\ E_o' \end{bmatrix} = \begin{bmatrix} R(\mathbf{p},\mathbf{e}) & R(\mathbf{s},\mathbf{e}) \\ R(\mathbf{p},\mathbf{o}) & R(\mathbf{s},\mathbf{o}) \end{bmatrix} \begin{bmatrix} E_{pi}' \\ E_{si}' \end{bmatrix} = S \begin{bmatrix} E_{pi}' \\ E_{si}' \end{bmatrix}, \tag{6}$$

where E_{si}' and E_{pi}' are the electric fields of the input **s** and **p** vectors in the isotropic medium, and E_e' and E_o' are the electric fields of the **e** and **o** vectors in the uniaxial medium, respectively. $R(\mathbf{p},\mathbf{e})$, $R(\mathbf{s},\mathbf{e})$, $R(\mathbf{p},\mathbf{o})$, and $R(\mathbf{s},\mathbf{o})$ are the transformation coefficients of the **p** to **e**, **s** to **e**, **p** to **o**, and **s** to **o** vectors, respectively, and S is the dynamic matrix at the interface. The optical propagation from an isotropic medium, through a uniaxial medium, to another isotropic medium is therefore given by

$$\begin{bmatrix} E_{po}' \\ E_{so}' \end{bmatrix} = J \begin{bmatrix} E_{pi}' \\ E_{si}' \end{bmatrix}, \tag{7}$$

where $J=S^{-1}GS$ is the Jones matrix, E_{so}' and E_{po}' are the electric fields of the output **s** and **p** vectors in the isotropic medium. The matrix G expresses the propagation of the ordinary and extraordinary waves across a homogeneous layer of thickness h as follows:

$$G = \begin{bmatrix} \exp(-iK_{ez}h) & 0 \\ 0 & \exp(-iK_{oz}h) \end{bmatrix}, \tag{8}$$

where K_{ez} and K_{oz} are the z components of the extraordinary and ordinary wave vectors, respectively. The propagation of the light inside the LC layer can then be approximated as

$$M = J_N J_{N-1} \cdots \cdot J_n \cdot \cdots J_2 J_1, \tag{9}$$

where N is the number of LC layer and is set to 50 in our simulation.

The color filters are modeled as absorptive and isotropic media. Their complex refractive index is expressed as

$$n_{\mathrm{CF}} = n - ik, \tag{10}$$

where n and k are the refractive index and extinction coefficient, which were already obtained from the optical characterizations of color filters.[1,2] The propagation matrix inside the color filter layer can then be expressed as

$$P_{\mathrm{CF}} = \begin{bmatrix} \exp(n_{\mathrm{CF}}Kd) & 0 \\ 0 & \exp(n_{\mathrm{CF}}Kd) \end{bmatrix}, \tag{11}$$

where K and d are the wave vector of the incident light and the thickness of the color filters, respectively. The interface between the color filters and LC can be expressed as the interface of two isotropic media as

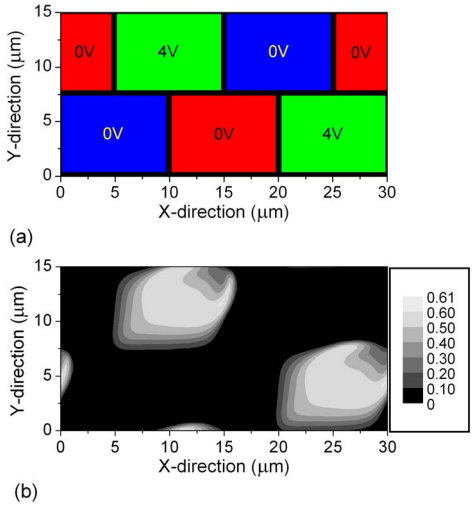

FIG. 3. (Color online) (a) The delta pixel arrangement and (b) the optical reflectance contour of a color pixel array at 550 nm wavelength.

$$D_{\mathrm{LC}\to\mathrm{CF}} = \begin{bmatrix} 2n_o/(n_{\mathrm{CF}}+n_o) & 0 \\ 0 & 2n_o/(n_{\mathrm{CF}}+n_o) \end{bmatrix}, \tag{12a}$$

and

$$D_{\mathrm{CF}\to\mathrm{LC}} = \begin{bmatrix} 2n_{\mathrm{CF}}/(n_o+n_{\mathrm{CF}}) & 0 \\ 0 & 2n_{\mathrm{CF}}/(n_o+n_{\mathrm{CF}}) \end{bmatrix}, \tag{12b}$$

where n_o is the ordinary refractive index of the LC mixture.

We modeled the reflection of the color LC cell by transmission through a LC cell, a color filter layer, and a mirrored LC cell in series. The overall optical behavior of the color LC cell with cross polarizers can then be expressed as

$$\begin{bmatrix} E_{po} \\ E_{so} \end{bmatrix} = P_o \cdot M(-\theta,\phi,-\Delta\varphi) \cdot D_{\mathrm{CF}\to\mathrm{LC}} \cdot P_{\mathrm{CF}} \cdot D_{\mathrm{LC}\to\mathrm{CF}} \cdot M(\theta,\phi,\Delta\varphi) \cdot P_i \cdot \begin{bmatrix} E_{pi} \\ E_{si} \end{bmatrix}, \tag{13}$$

where $P_i=\left(\begin{smallmatrix}1&0\\0&0\end{smallmatrix}\right)$ and $P_o=\left(\begin{smallmatrix}0&0\\0&1\end{smallmatrix}\right)$ are matrix representations of the ideal input and output polarizers. E_{pi} and E_{si} are electric fields of the incident **p** and **s** vectors, and E_{po}' and E_{so}' are electric fields of the output **p** and **s** vectors, respectively. $M(\theta,\phi,\Delta\varphi)$ and $M(-\theta,\phi,-\Delta\varphi)$ represent the propagation matrices through the first and mirrored LC cells, respectively. The reflectance of the color LC cell is therefore

$$R = \frac{|E_{so}|^2 + |E_{po}|^2}{|E_{si}|^2 + |E_{pi}|^2}. \tag{14}$$

Equation (14) gives the one-dimensional (1D) optical reflectance of the color LC cell. With the 3D director obtained from the LC electromechanical analysis, we proceeded to integrate the 1D reflectance through each vertical rectangular mesh of the 3D director and obtained the 3D optical reflectance.

We arranged the color pixel array in a delta shape and turned on green pixels as shown in Fig. 3(a). The subpixel was 10 μm by 7.5 μm for a pixel pitch of 15 μm. We simulated a 550 nm light into this pixel array and calculated for its optical reflectance. Figure 3(b) shows contours of the

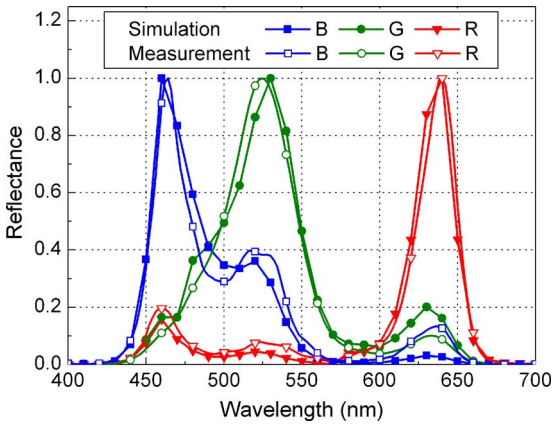

FIG. 4. (Color online) The simulated and measured optical reflectances of the color pixel array in the visible spectrum.

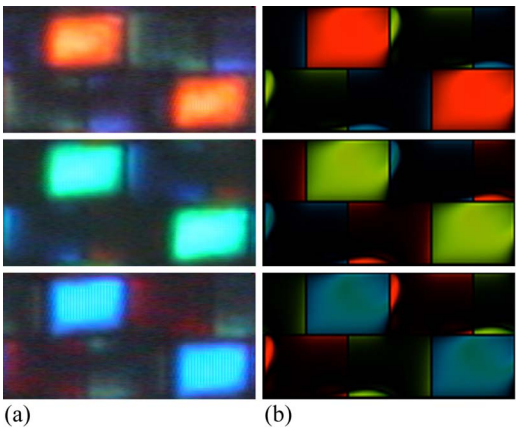

FIG. 5. (Color online) (a) The observed and (b) simulated color pixels of the MTN CF-LCOS microdisplay.

simulated optical reflectance of the pixel array. The total optical reflectance at this wavelength could also be obtained by integration of the reflectance over the pixel array.

We varied the wavelength of the illuminating light for the entire visible spectrum from 400 to 700 nm, and integrated the optical reflectance over the pixel array. Figure 4 shows the simulated total optical reflectance of the color pixel array in the visible spectrum. We have fabricated a CF-LCOS microdisplay of the same pixel size and LC mode. Figure 4 also shows the measured optical reflectance of this microdisplay by a spectral radiometer. The measurements were performed under a microscope with a long focal lens and red, green, and blue light-emitting diode (LED) light sources, respectively. For a fair comparison, we also used these LED light sources for calculations of the optical reflectance. The normalized simulated and measured optical reflectances agreed with each other very well.

C. sRGB representation of color pixels

The optical reflectance analysis can reveal important monochrome parameters, including reflectivity and contrast. The optical reflectance analysis of color LC cells further carries important color parameters. We converted the optical reflectance spectrum to the CIE 1931 color space[10] for color coordinate as follows:

$$\begin{bmatrix} X \\ Y \\ Z \end{bmatrix} = C \int_{380}^{780} R(\lambda) S(\lambda) \begin{bmatrix} \bar{x}(\lambda) \\ \bar{y}(\lambda) \\ \bar{z}(\lambda) \end{bmatrix} d\lambda, \tag{15}$$

where λ is the wavelength, $R(\lambda)$ is the spectral reflection factor and $S(\lambda)$ is the spectrum of backlight. $\bar{x}(\lambda)$, $\bar{y}(\lambda)$, and $\bar{z}(\lambda)$ are color-matching functions for the CIE standard colormetric system, and C is a constant and can be obtained by

$$C = \frac{100}{\int_{380}^{780} S(\lambda)\bar{y}(\lambda) d\lambda}. \tag{16}$$

This color coordinate was a good measure of color purity of the display. But it lacked of spatial information to illustrate which part of the pixels caused leakage and degraded the color.

In an attempt to visualize the color fringing field among small color pixels, we expressed the optical reflectance in sRGB format in the pixel array. The conversion from the CIE 1931 color space to the sRGB representation was as follows:

$$\begin{bmatrix} R_{\mathrm{sRGB}} \\ G_{\mathrm{sRGB}} \\ B_{\mathrm{sRGB}} \end{bmatrix} = \begin{bmatrix} 3.2410 & -1.5374 & -0.4986 \\ -0.9692 & 1.8760 & 0.0416 \\ 0.0556 & -0.2040 & 1.0570 \end{bmatrix} \begin{bmatrix} X \\ Y \\ Z \end{bmatrix}_{D65}. \tag{17}$$

Figure 5 shows the observed and simulated color pixels of the MTN CF-LCOS microdisplay. The simulated spatial color images matched the observed ones very well. The bright pixels were fully on and there was no dark spot within the bright pixels. But the dark pixels leaked on four sides due to the lateral fringing field, and the main leakage was on the right-side adjacent to the bright pixels.

III. OPTIMIZATIONS

We have developed a 3D optical modeling of small color pixels in reflective twisted nematic cells, and have verified the accuracy of this modeling with experiments. With this 3D optical analysis as a tool, we were able to locate more efficiently the color leakage in the pixel array and minimize the color fringing field accordingly. There are many factors that could affect the color fringing field. For example, arrangement of subpixels in strip, delta, or mosaic shapes would disperse the fringing field in different extents. The change of rubbing directions with respect to the pixel edges could move the leakage around. Alternation of thickness or dielectric constant of color filters would redistribute the fringing field. Different pixel size could affect relatively the color leakage. But the most important design parameter was still on the application specific LC mode. The color leakage could be minimized at a particular LC mode even at a very small pixel size. In this section, we minimized the fringing field in small color pixels by pixel arrangement, rubbing direction, and LC mode. In the next section, we compared the color purity and reflectivity of the pixel array with respect to pixel size and thickness of color filters.

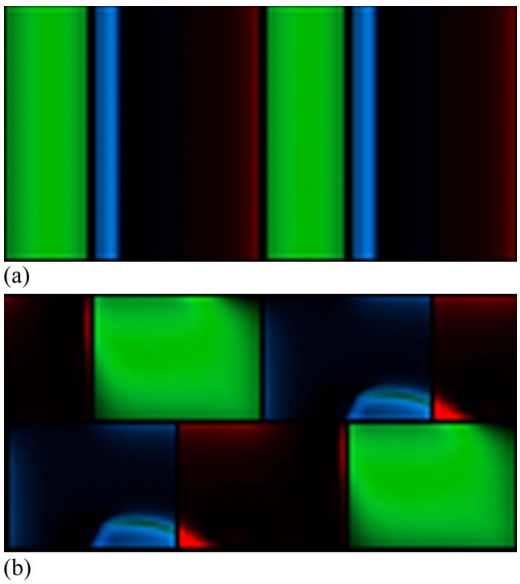

FIG. 6. (Color online) The simulated spatial optical reflectance of (a) the strip and (b) delta pixels when the green pixels were turned on.

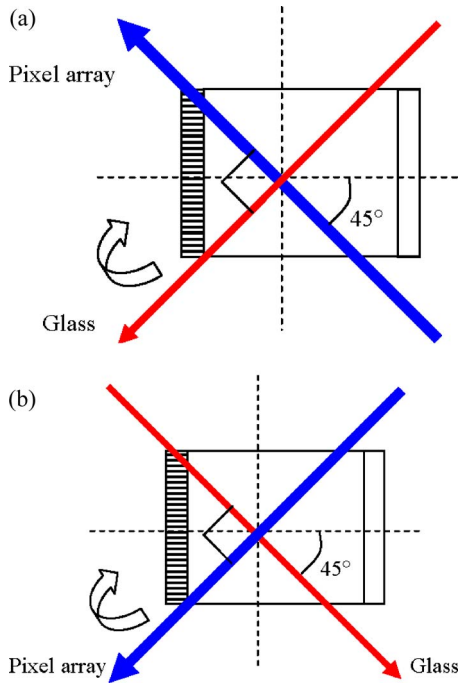

FIG. 7. (Color online) (a) The normal and (b) optimized rubbing schemes.

A. Pixel arrangement

We arranged the color pixels in strip and delta shapes and performed the 3D optical analyses of these two pixel structures. Both the structures used the same MTN mode and had a same pixel pitch of 15 μm. Whereas, the subpixel pitch was 15 μm by 5 μm for the strip shape and 10 μm by 7.5 μm for the delta shape. The pixel gap was 0.5 μm in both cases. Figure 6 shows the spatial optical reflectance of both the pixel arrangements in which the green pixels were turned on. The leakage occurred more on the blue pixels than on the red pixels in both the arrangements. However, it was clearly noted that the strip pixels had more leakage than the delta ones.

The dark blue pixels in the strip pixels had a leakage, which occupied more than 30% of the pixel area, while the dark blue pixels in the delta pixels had a smaller leakage. As a result, the color purity of the strip pixels was worse than that of the delta ones. We obtained a green color purity of (0.224, 0.492) for the strip pixels and (0.241, 0.560) for the delta ones from the simulations. The green delta pixels had a larger y value in the color coordinate, and hence a better green color. Similarly, we simulated for the red and blue images, and obtained the red and blue color purities of (0.572, 0.351) and (0.179, 0.219), respectively, for the strip pixels, and (0.601, 0.325) and (0.157, 0.205), respectively, for the delta pixels. Again, the delta pixels had better red and blue colors than that of the strip pixels. In addition to a better color purity, it should be noted that the delta pixels had a larger feature size of 7.5 μm in comparison with 5 μm of the strip pixels, and hence easier for color filter processing.

B. Rubbing direction

The rectangular or square pixels had finite area and pixel edges. The rubbing direction with respect to the pixel edges could produce different degree of color leakage in the finite pixel area. There should be an optimized rubbing direction for a least color leakage. However, the rubbing direction had to be related to the LC mode and optical axis of the light path. It could not be any arbitrary angle, otherwise, the projection or viewing image would not be landscape or portrait. In this regard, there were only two possible rubbing directions, which were rotated by 90° of each other.

In the simulation of the delta pixels in Fig. 6(b), the rubbing directions on the pixel array and the top glass plate were shown in Fig. 7(a). The rubbing direction on the pixel array was 45° counterclockwise of the optical axis, and the rubbing direction on the top glass plate was 45° clockwise of the optical axis. We rotated the rubbing directions by 90° counterclockwise as shown in Fig. 7(b) and performed the 3D optical analysis of this new structure.

Figure 8 shows the spatial optical reflectance of the same delta pixels but with two different rubbing directions as illustrated in Fig. 7. Again, we first illustrated the green image in which the green pixels were turned on, while the red and blue pixels were turned off. It was clearly seen that the color leakage was moved from the long side of the dark pixels to the short side of the dark pixels as the rubbing directions were rotated by 90°. Figure 8(a) had the color leakage penetrated more on the long side of the dark pixels, while Fig. 8(b) had the color leakage penetrated more on the short side of the dark pixels. As a result, the area of color leakage was accordingly reduced in Fig. 8(b). It was found that the green color purity was improved from (0.241, 0.560) to (0.247, 0.585) when the color leakage was moved from the long to the short side of the dark pixels. Similarly, the red and blue color purities were also improved from (0.601, 0.325) and (0.157, 0.205) to (0.602, 0.310) and (0.148, 0.207), respectively.

C. Liquid-crystal mode

In addition to the MTN mode, there are other mixed twisted nematic and birefrigence (MTB) modes[11] that are

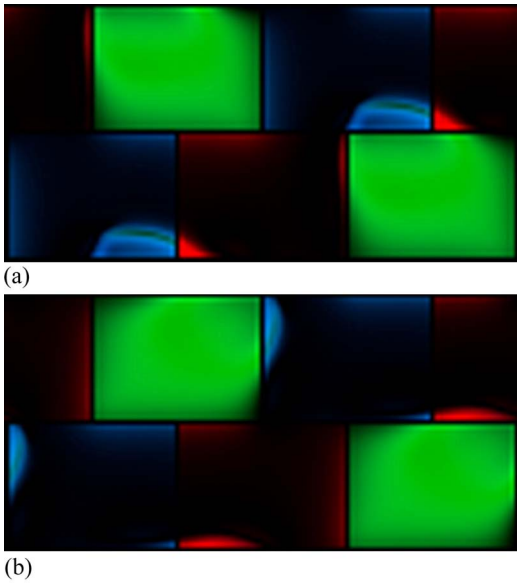

FIG. 8. (Color online) The simulated spatial optical reflectance of the delta pixels in (a) the normal and (b) optimized rubbing schemes.

suitable for the CF-LCOS microdisplays. We did a systematic search of these MTB modes and found that some of these modes had very low color leakage. Figure 9 shows the spatial optical reflectance of the optimized MTN mode and a low-leakage MTB mode, which had an 80° twist angle, an 18° polarizer angle, a 2° pretilt angle, and a 0.25 retardation. Again, we rubbed the low-leakage MTB mode properly, so the color leakage appeared on the short side of the pixels. The green color purity was further improved from (0.247, 0.585) of the optimized MTN mode to (0.243, 0.601) of the low-leakage MTB mode. Similarly, the red and blue color purities were also improved from (0.602, 0.310) and (0.148, 0.207) to (0.641, 0.308) and (0.136, 0.182), respectively.

It was observed from Fig. 9. that the bright green pixels of this low-leakage MTB mode were also shrunk slightly to

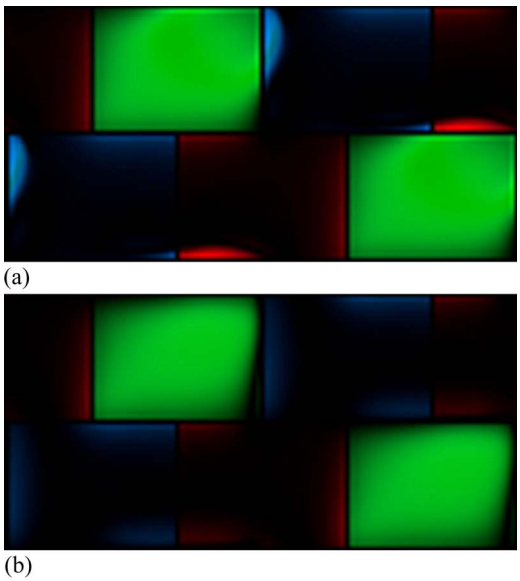

FIG. 9. (Color online) The simulated spatial optical reflectance of (a) the optimized MTN mode and (b) a low-leakage MTB mode.

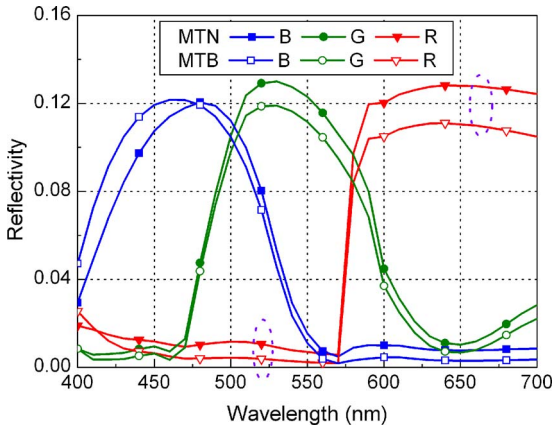

FIG. 10. (Color online) The simulated reflectivity of the color images for both the color MTN and MTB LC cells.

a smaller area. As a result, the peak reflectivity of the green image was slightly reduced from 13.0% in the MTN mode to 11.9% in the low-leakage MTB mode as shown in Fig. 10. That is to say, the reflectivity or brightness of color images was traded slightly for a better color saturation. However, it should be noted that the overall brightness of the pixel array, when all the pixels are turned on, remains the same because there is no color fringing field when all the red, green, and blue pixels are of the same voltage. Figure 11 shows the simulated reflectivity of the white image for both the color MTN and MTB cells. The reflectivity of the white image in Fig. 11 was much larger than the reflectivity of the color images in Fig. 10 because there was no lateral fringing field in the white image. Both the reflectivity curves in Fig. 11 were similar to each other because both the MTN and MTB modes were high-reflectivity twisted nematic modes.[12] The reflectivity curves of the white image mainly revealed the transmission characteristics of color filters.

The overall reflectivity of the white image with a D65 light source was almost the same and was 22% and 22.1%, respectively, for the color MTN and MTB cells, respectively. Here, we defined the overall reflectivity of the white image as

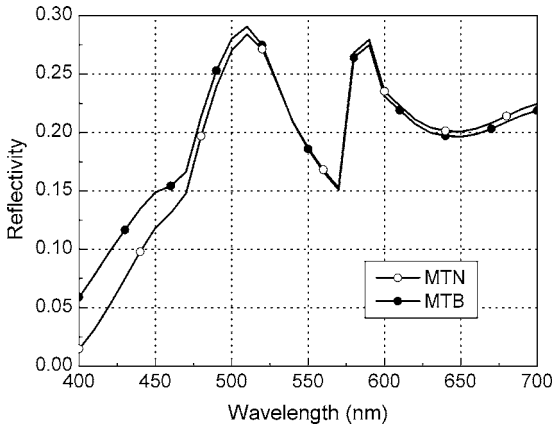

FIG. 11. The simulated reflectivity of the white image for both the color MTN and MTB LC cells.

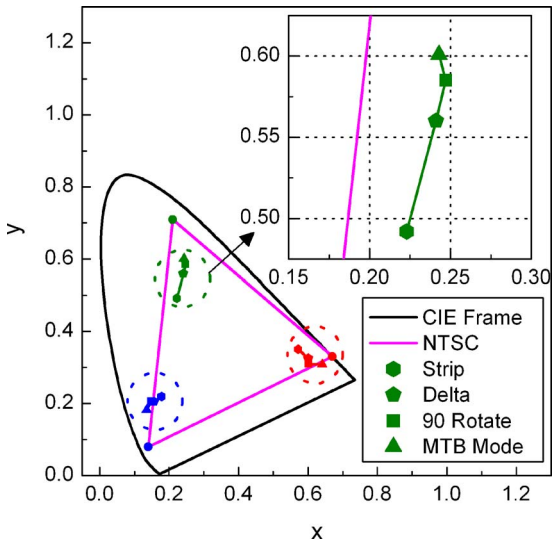

FIG. 12. (Color online) The improvement of color with respect to the pixel arrangement, rubbing direction, and LC mode in the CIE 1931 color space.

$$R_{D65} = \frac{\int_{400}^{700} R_{\text{white}}(\lambda) L_{D65}(\lambda) V(\lambda) d\lambda}{\int_{400}^{700} L_{D65}(\lambda) V(\lambda) d\lambda}, \tag{18}$$

where $R_{\text{white}}(\lambda)$ is the spectral reflectivity of the white MTB image as obtained in Fig. 11, $L_{D65}(\lambda)$ is the normalized luminance of the D65 light source, and $V(\lambda)$ is the photonic luminous efficiency function.

D. Summary of the optimizations

In this section, we have varied the pixel arrangement, rubbing direction, and LC mode to minimize the fringing field and improve the color purity of the CF-LCOS microdisplays. The color purity was improved from 32% NTSC level of the strippixels to 47% of the delta pixels, to 56% of the optimal rubbing direction, and to 63% of the low-leakage MTB mode as shown in Fig. 12. These improvements of color purity were obtained without sacrifice or without too much sacrifice of the reflectivity or brightness of the individual color. The (on) region of the bright pixel still occupied most of the pixel area and therefore, the reflectivity of each color pixel was still high and ranged from 40% to 50%. Because each color occupies one-third of the pixel array, the peak reflectivity of the pixel array, or the CF-LCOS microdisplay was therefore 11.9%, 12.2%, and 11.1%, respectively, for the red, green, and blue images as already shown in Fig. 10.

IV. PIXEL SIZE AND THICKNESS OF COLOR FILTERS

In this section, we discuss the relation of color fringing field with respect to pixel size and thickness of color filters. These two parameters can affect the color, reflectivity, contrast, and other properties of the CF-LCOS microdisplays. The optimization of pixel size and thickness of color filters should be compromised among these display properties for specific applications.

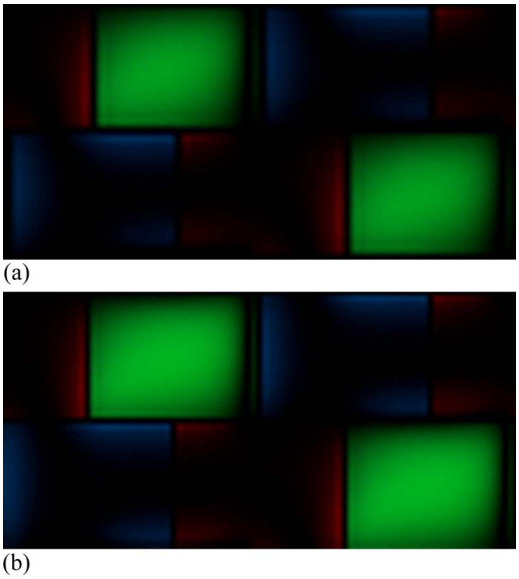

FIG. 13. (Color online) The simulated spatial optical reflectance of the small (a) 9 and (b) 12 μm pixels.

A. Pixel size

In order to have high resolution for this spatial color microdisplay, pixels have to be very small. We further applied the 3D optical analysis to study the color fringing field with respect to pixel size. Figure 13 shows the spatial optical reflectance of small pixels, which had a pixel pitch of 12 and 9 μm, respectively. The color leakage into the dark pixels should be more or less the same, but its percentage of penetration was relatively increased for a smaller pixel. As a result, the green color purity was also slightly reduced from (0.243, 0.601) of the 15 μm pixels to (0.233, 0.587) of the 12 μm and to (0.231, 0.577) of the 9 μm pixels. Similarly, the red and blue color purities were also reduced slightly from (0.641, 0.308) and (0.136, 0.182) of the 15 μm pixels to (0.615, 0.310) and (0.139, 0.175) of the 12 μm and to (0.597, 0.309) and (0.141, 0.172) of the 9 μm pixels, respectively.

While the color purity was reduced due to a relatively larger color leakage in the smaller pixel, the ON or color region of the smaller bright pixel was also reduced. The peak reflectivity of the green image was reduced from 11.9% of the 15 μm pixels to 8.4% of the 12 μm and to 6.1% of the 9 μm pixels as shown in Fig. 14. The reflectivity of the red and blue pixels also followed a similar reduction. However, it should be noted that the overall brightness of the pixel array had no change because there was no color fringing field when all the red, green, and blue pixels were turned on and of the same voltage. The reduction in the pixel size would not affect the overall panel reflectivity, but only the color saturation and brightness of individual color.

We have fabricated a CF-LCOS microdisplay of 1280 $\times$768$\times$RGB spatial resolution with a pixel pitch of 15 μm. The display area was 0.87″ in diagonal. By reducing the pixel size from 15 to 10 μm, we shall be able to design and fabricate a CF-LCOS microdisplay of 1920$\times$1080$\times$RGB spatial resolution with about the same display area of 0.87″

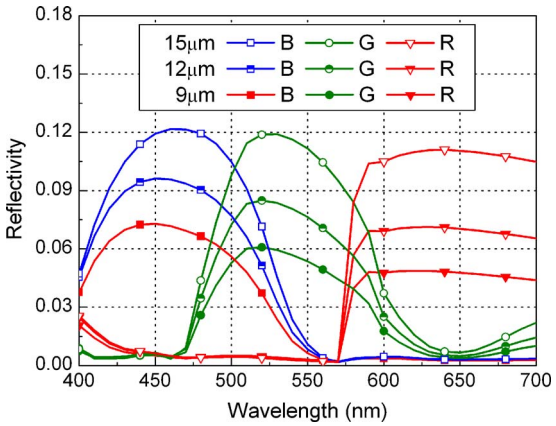

FIG. 14. (Color online) The simulated reflectivity of the green image for the small pixels of 9, 12, and 15 μm pitch.

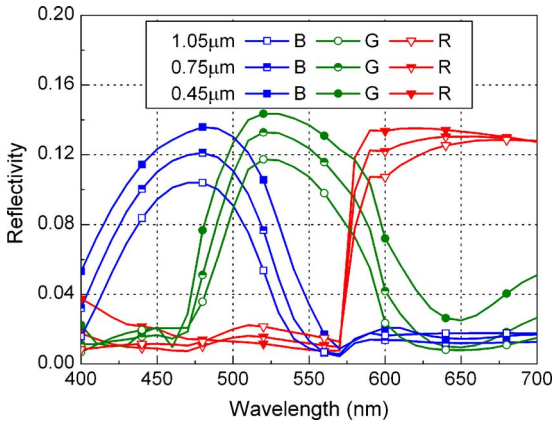

FIG. 15. (Color online) The simulated reflectivity of a color MTN pixel array with different thickness of color filters.

in diagonal. This 1080p high-definition television (HDTV) display should still maintain a good color and high reflectivity according to the simulations.

B. Thickness of color filters

The reduction of pixel size would affect mainly the lateral electric field and color; it would not affect the vertical electric field across the color filter and LC layers, and hence the contrast of the display remains the same. The alternation of thickness of color filters would affect both the lateral and vertical electric fields, and hence the change of the display properties is more complicated. A thinner color filter would reduce the purity of the colored light through the color filters, but it would also allow more voltage across the LC layer for a better contrast. The color saturation of the display was mainly determined by the colored light and contrast. There should be an optimal thickness of color filters, at which the purity of the colored light and the contrast were compromised for a good color display.

Our guideline of the thickness of color filters in the reflective CF-LCOS microdisplays was half of the thickness of color filters in the transmittive thin film transistor liquid crystal display (TFT-LCD) displays because the light passed through the color filters twice in the reflective CF-LCOS microdisplays. With this guideline, we have specified the thickness of color filters at 0.75 μm and have developed a color filter process to obtain a uniform 0.75 μm color filter array.[1,2] We have also used this thickness for all the optical simulations before. But the thickness of color filters is a parameter that we can control and alter.

We varied the thickness of color filters from 0.45, 0.6, 0.75, and 0.9 to 1.05 μm in the color LC cells and simulated for their color coordinates with the 3D optical analysis. Figure 15 shows the simulated reflectivity of the color pixel array configured in the MTN mode. It was noted that the reflectivity was proportionally reduced with the increased thickness of color filters. The peak reflectivity of the green image was reduced from about 14.4% at 0.45 μm thickness of color filters to 13.0% at 0.75 μm, and to 11.7% at 1.05 μm thickness of color filters.

Figure 16 shows the simulated color coordinates of the MTN CF-LCOS microdisplays with different thickness of color filters in the CIE 1931 color space. The color purity was improved greatly from 36% NTSC level at 0.45 μm thickness of color filters to 46% at 0.6 μm and to 51% at 0.75 μm thickness of color filters. The further increase of the thickness of color filters to 0.90 μm did not increase the color saturation of the cells. The color saturation was actually reduced to 43% NTSC level when the thickness of color filters was increased to 1.05 μm. At this thickness, 45% of the applied voltage was dropped in the color filters and hence the voltage across the LC layer was not large enough to have a good contrast. The color saturation was therefore reduced.

V. CONCLUSION

We have developed a 3D optical modeling of fringing field in small and reflective color pixels. The optical modeling includes a LC electromechanical analysis and an optical reflectance calculation. The simulated optical reflectance was expressed in both the color coordinate and in the pixel array, so it was easier to quantify and locate the color leakage. The simulated optical reflectance agreed well with the experimental ones. With this 3D optical analysis as a tool, we could minimize the color fringing field with respect to the pixel arrangement, rubbing direction, and LC mode. The color pu-

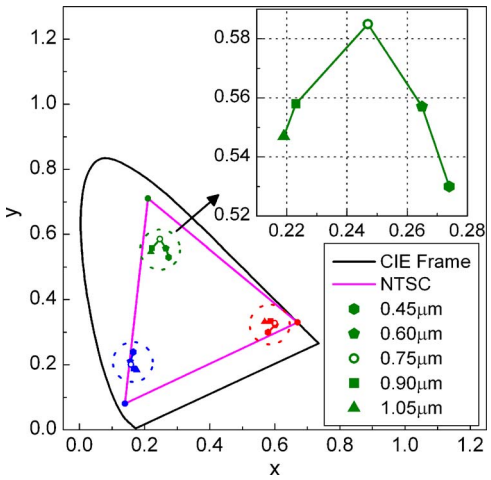

FIG. 16. (Color online) The simulated color of a color MTN pixel array in the CIE 1931 color space with different thickness of color filters.

rity was improved from 32% NTSC level of the strip pixels to 47% of the delta pixels, to 51% of the optimal rubbing direction, and to 63% of the low-leakage MTB mode. The relation of the color fringing field with pixel size and thickness of color filter were also studied. The color purity was generally reduced when the pixel size was reduced. But with a low-leakage LC mode, the color purity could still be maintained at 54% NTSC level even when the pixel size was reduced to 9 μm. This suggested that the CF-LCOS microdisplays were feasible for very high-resolution display applications.

ACKNOWLEDGMENT

This work was sponsored partly by grants from the Research Grant Council of the Government of the Hong Kong Special Administrative Region.

[1]H. C. Huang, B. L. Zhang, H. S. Kwok, P. W. Cheng, and Y. C. Chen, SID Int. Symp. Digest Tech. Papers **36**, 880 (2005).
[2]B. L. Zhang, H. J. Peng, H. C. Huang, and H. S. Kwok, SID Int. Symp. Digest Tech. Papers **36**, 1302 (2005).
[3]H. C. Huang, D. D. Huang, and J. Chen, Jpn. J. Appl. Phys., Part 1 **39**, 485 (2000).
[4]Refer to http://www.color.org/sRGB.html
[5]J. E. Anderson, P. E. Watson, and P. J. Bos, *LC3D: Liquid Crystal Display 3-D Director Simulator Software* (Artech House, Norwood, MA, 2001), Pt. 1.
[6]A. Lien, Appl. Phys. Lett. **62**, 1079 (1993).
[7]S. Dickmann, J. Eschler, O. Cossalter, and D. Mlynski, SID Int. Symp. Digest Tech. Papers **24**, 638 (1993).
[8]S. T. Wu and C. S. Wu, Appl. Phys. Lett. **68**, 1455 (1996).
[9]C. Gu and P. Yeh, J. Opt. Soc. Am. A **10**, 966 (1993).
[10]G. Wyszecki and W. S. Stiles, *Color Science: Concepts and Methods, Quantitative Data and Formulae* (Wiley, New York, 1982), Chap. 3.
[11]J. Chen, P. W. Cheng, S. K. Kwok, C. S. Li, S. Young, H. C. Huang, and H. S. Kwok, SID Int. Symp. Digest Tech. Papers **30**, 754 (1999).
[12]J. Chen, F. H. Yu, H. C. Huang, and H. S. Kwok, J. Soc. Inf. Disp. **7**, 127 (1999).